Characterizing the Response of Calcium Signal Transducers to Generated Calcium Transients†

Jonathan P. Davis,‡ Svetlana B. Tikunova,‡ Michael P. Walsh,§ and J. David Johnson*,‡

Department of Medical Biochemistry, The Ohio State University Medical Center, Columbus, Ohio 43210, and Department of Medical Biochemistry, University of Calgary, Calgary, Alberta T2N 4NI, Canada

Received October 19, 1998; Revised Manuscript Received January 25, 1999

ABSTRACT: Cellular Ca^{2+} transients and Ca^{2+}-binding proteins regulate physiological phenomena as diverse as muscle contraction, neurosecretion, and cell division. When Ca^{2+} is rapidly mixed with slow Ca^{2+} chelators, EGTA, or Mg^{2+}/EDTA, artificial Ca^{2+} transients (ACTs) of varying duration (0.1−50 ms half-widths (hws)) and amplitude can be generated. We have exposed several Ca^{2+} indicators, Ca^{2+}-binding proteins, and a Ca^{2+}-dependent enzyme to ACTs of various durations and observed their transient binding of Ca^{2+}, complex formation, and/or activation. A 0.1 ms hw ACT transiently occupied ∼70% of the N-terminal regulatory sites of troponin C consistent with their rapid Ca^{2+} on-rate ($8.7 \pm 2.0 \times 10^7$ M^{-1} s^{-1}). A 1.1 ms hw ACT produced ∼90% transient binding of the N-terminal of calmodulin (CaM) to the RS-20 peptide, but little binding of CaM's C-terminal to RS-20. A 0.6 ms hw ACT was sufficient for the N-terminal of CaM to transiently bind ∼60% of myosin light chain kinase (MLCK), while a 1.8 ms hw ACT produced ∼22% transient activation of the sarcoplasmic reticulum (SR) Ca^{2+}/ATPase. In both cases, the ACT had fallen back to baseline ∼10−30 ms before maximal binding of CaM to MLCK or SR Ca^{2+}/ATPase activation occurred and binding and enzyme activation persisted long after the Ca transient had subsided. The use of ACTs has allowed us to visualize how the Ca^{2+}-exchange rates of Ca^{2+}-binding proteins dictate their Ca^{2+}-induced conformational changes, Ca^{2+}-induced protein/peptide and protein/protein interactions, and enzyme activation and inactivation, in response to Ca^{2+} transients of various amplitude and duration. By characterizing the response of these proteins to ACTs, we can predict with greater certainty how they would respond to natural Ca^{2+} transients to regulate cellular phenomena.

Ca^{2+} is a ubiquitous second messenger responsible for regulating a large variety of cellular processes (*1*). In cells, [Ca^{2+}] rises in a transient fashion, allowing for the activation and subsequent inactivation of various Ca^{2+}-binding proteins and Ca^{2+}-regulated enzymes. The Ca^{2+}-exchange rates of Ca^{2+}-binding proteins are variable (for review, see ref *2*), allowing them to be "tuned" so that they are activated to a specific extent and for a particular duration by cellular Ca^{2+} transients. Alterations in the profile of Ca^{2+} transients or in the kinetics of Ca^{2+} exchange with Ca^{2+}-binding proteins can produce dramatic changes in Ca^{2+}-dependent physiological responses.

Fluorescent Ca^{2+} indicators, such as fluo-3 and mag-fura-2 (MF2),[1] allow the time course of Ca^{2+} transients to be followed within living cells. The half-widths (hws) of Ca^{2+} transients vary greatly from ∼1 ms in neurons (*3*) to ∼15 ms in skeletal muscle (*4*) and up to minutes in smooth muscle (*5*). Cytosolic [Ca^{2+}] typically rises in cells when hormonal or neuronal stimulation triggers the entry of extracellular Ca^{2+} and/or the release of Ca^{2+} from internal stores (endoplasmic or sarcoplasmic reticulum (ER, SR)) (*6, 7*). Cytosolic [Ca^{2+}] decreases as Ca^{2+}/ATPases pump Ca^{2+} into the ER or SR or extrude Ca^{2+} across the plasma membrane. When Ca^{2+} uptake mechanisms fail, Ca^{2+} transients are prolonged and this can lead to cell necrosis and cell death (*8*). A transient rise in intracellular [Ca^{2+}] plays a fundamental role in activating various Ca^{2+}-binding proteins and Ca^{2+}-regulated enzymes which are essential for cardiac, skeletal, and smooth muscle contraction, neurotransmission, energy metabolism, cell cycling, and growth (*9*).

Nature has developed a variety of mechanisms to modify both the amplitude and the duration of the Ca^{2+} transient in order to evoke specific cellular responses. For example, β-adrenergic agonists increase the amplitude and shorten the duration of the Ca^{2+} transient in cardiac ventricular muscle, causing increased contractility and faster relaxation (*10*). Thus, the amplitude and duration of the Ca^{2+} transient can dictate the extent and longevity of Ca^{2+} binding to proteins and subsequent enzyme activation. It has also been shown

† This work was supported by grants from The National Institutes of Health (DK33727 to J.D.J.), Medical Research Council of Canada (to M.P.W.), and a Medical Scientist Award from the Alberta Heritage Foundation for Medical Research (to M.P.W.).

* Address correspondence to Dr. J. David Johnson, Department of Medical Biochemistry, The Ohio State University Medical Center, 333 Hamilton Hall, 1645 Neil Ave., Columbus, OH 43210-1218. Phone: 614-292-4762. Fax: 614-292-4118. E-mail: johnson.52@osu.edu.

‡ The Ohio State University Medical Center.

§ University of Calgary.

[1] Abbreviations: MF2, mag-fura-2; hw, half-width; ER, endoplasmic reticulum; SR, sarcoplasmic reticulum; TnC, troponin C; TnC-danz, dansylaziridine labeled troponin C; TBQ, 2,5-di-(*tert*-butyl)-1,4-benzohydroquinone; CaM, calmodulin; MLCK, myosin light chain kinase; RS-20, smooth muscle myosin light chain kinase peptide (ARRKWQKTGHAVRAIGRLSS); MIANS, 2-(4′-maleimidoanilino)-naphthalene-6-sulfonic acid; ACT, artificial Ca^{2+} transient; TNP/ATP, 2′,3′-*O*-(2,4,6-trinitrophenyl)/ATP.

10.1021/bi982495z CCC: $18.00
Published on Web 03/12/1999

in B lymphocytes that Ca^{2+} transients of different amplitude and duration control the differential activation of specific transcriptional regulators (*11*). These studies imply that the tuning of Ca^{2+} binding to proteins is also an important mechanism to alter cellular responses to changes in $[Ca^{2+}]$. Another example of this tuning mechanism is observed in fast twitch skeletal muscle. During a twitch, Ca^{2+} rapidly binds to the N-terminal regulatory sites of troponin C (TnC) to elicit a contraction, while Ca^{2+} slowly exchanges with the Ca^{2+} buffering protein parvalbumin to aid relaxation (*12*). Thus, modifications of both the Ca^{2+}-transient and Ca^{2+}-exchange properties of Ca^{2+}-binding proteins can produce alterations in cell function.

Naturally occurring Ca^{2+} transients can be modified by varying electrical stimulation parameters (*13*), by drugs that inhibit Ca^{2+} resequestration into cellular compartments (*14*, *15*), or by addition of extracellular (*14*) or intracellular (*13*, *16*) Ca^{2+} chelators such as EGTA. These modifications have helped to determine the role Ca^{2+} plays in physiological systems. For example, in living skeletal muscle at 10 °C, intracellular EGTA caused a 2-fold decrease in the hw of twitch-induced Ca^{2+} transients, while the SR Ca^{2+}/ATPase inhibitor 2,5-di-(*tert*-butyl)-1,4-benzohydroquinone (TBQ) caused a 2-fold increase in the hw of the Ca^{2+} transient (*13*). As the duration of the Ca^{2+} transient was increased from ~40 to 130 ms, there was a linear increase in tension development. Thus, the duration of the Ca^{2+} transient in skeletal muscle is a primary determinant of force.

In these studies we show that, when Ca^{2+} chelators with slow Ca^{2+} on-rates (EGTA and Mg^{2+}/EDTA) are rapidly mixed with Ca^{2+}, the $[Ca^{2+}]$ initially rises and then falls as these chelators bind Ca^{2+}. This allowed us to generate Ca^{2+} transients of various amplitudes and durations in a stopped-flow apparatus and to determine the response of Ca^{2+} indicators (fluo-3 and MF2), Ca^{2+}-binding proteins (calmodulin (CaM) and TnC), and Ca^{2+}-dependent enzymes (myosin light chain kinase (MLCK) and SR Ca^{2+}/ATPase) to these Ca^{2+} transients. Previously investigators determined Ca^{2+} on-rates by rapidly mixing Ca^{2+} with an apo Ca^{2+}-binding protein and determined Ca^{2+} off-rates by mixing a Ca^{2+} chelator with a Ca^{2+}-saturated Ca^{2+}-binding protein. Our new approach allows us to follow the consequences of both Ca^{2+} binding and Ca^{2+} removal on the following: Ca^{2+}-induced conformational changes; Ca^{2+}-induced protein/peptide and protein/protein interactions; and enzyme activation and inactivation, in response to Ca^{2+} transients of various amplitude and duration. This has enabled us to define how these Ca^{2+}-binding proteins and Ca^{2+}-dependent enzymes are tuned to receive and transduce the Ca^{2+} signal into cellular actions. This approach should further our understanding of how cellular Ca^{2+} transients regulate Ca^{2+}-dependent processes.

EXPERIMENTAL PROCEDURES

Materials. Quin-2, mag-fura-2, fluo-3, and TNP/ATP were purchased from Molecular Probes (Eugene, OR); EDTA and EGTA were purchased from Sigma (St. Louis, MO); and hydroxylapatite was purchased from Bio-Rad (Hercules, CA). RS-20, smooth muscle myosin light chain kinase CaM-binding peptide (ARRKWQKTGHAVRAIGRLSS), was purchased from American Peptide Co. (Sunnyvale, CA). All other chemicals were of analytical grade.

Table 1

complexes	K_{on} on-rate (M^{-1} s^{-1})	K_{off} off-rate (s^{-1})	K_d affinity (M)
EGTA + Ca^{2+}	1.3×10^6	0.55	4.2×10^{-7}
EDTA + Ca^{2+}	2.2×10^7	0.7	3.2×10^{-8}
EDTA + Mg^{2+}	8.75×10^5	2.8	3.2×10^{-6}
MF2 + Ca^{2+}	2×10^8	4000	2×10^{-5}
Fluo-3 + Ca^{2+}	5.4×10^8	170	3.2×10^{-7}
TnC N-terminal + Ca^{2+}	8.7×10^7	160	1.8×10^{-6}
CaM C-terminal + Ca^{2+}	2.3×10^6	2.4	1×10^{-6}
CaM N-terminal + Ca^{2+}	1.6×10^8	405	2.5×10^{-6}
CaM N-terminal + Ca^{2+} + MLCK	6.7×10^7	0.031	5×10^{-10}

Protein Purification. CaM was purified from bovine brain and wheat germ as described previously by Kasturi et al. (*17*). Wheat germ CaM and skeletal TnC were fluorescently labeled with 2-(4′-maleimidoanilino)-naphthalene-6-sulfonic acid (MIANS) (*17*) and dansylaziridine (DANZ) (*18*), respectively. MLCK was purified to electrophoretic homogeneity from chicken gizzard smooth muscle as described by Ngai et al. (*19*). SR vesicles were prepared from the back and leg muscles of rabbits by the method of Elter and Inesi (*20*).

Methods. Kinetic measurements were performed by mixing an equal volume (50 μL) of each solution together in an Applied Photophysics Ltd. (Leatherhead, U.K.) model SF.17 MV stopped-flow instrument which has a dead time of 1.6 ms. The samples were excited using a 150 W Xenon arc source at the specified wavelength. Fluorescence emission was monitored through the specified interference filters. The curve fitting program (by P. J. King, Applied Photophysics Ltd.) uses the nonlinear Levenberg−Marquardt algorithm. The calibration of the change in quin-2 fluorescence into moles of Ca^{2+} dissociating from the Ca^{2+}/CaM/RS-20 complex was previously described by Johnson et al. (*21*).

Computer Modeling. Computer simulations were performed using KSIM version 1.1 (N. C. Millar, UCLA School of Medicine, Los Angeles, (*22*)), which solved a set of differential equations numerically using the Runge−Kutta method. All reactions were considered to be bimolecular, with kinetic parameters (association and dissociation rates) corresponding to those of the experimental data as listed in Table 1 and the appropriate figure legends. The initial concentrations of the reagents in the simulations were set at the steady-state values corresponding to the contents of the two stopped-flow syringes immediately after mixing (time = 0).

RESULTS

Response of a Rapid and Slow Ca^{2+} Indicator to a 1.2 ms hw Artificial Ca^{2+} Transient. Since EGTA has a slow Ca^{2+} on-rate, when Ca^{2+} is rapidly mixed with EGTA, free $[Ca^{2+}]$ initially rises and then falls as it is chelated by EGTA. The slow Ca^{2+} chelation by EGTA thereby allows the production of artificial Ca^{2+} transients (ACTs) in a stopped-flow apparatus. The KSIM computer program (*22*) was used to simulate the Ca^{2+} transient which would be produced when 100 μM Ca^{2+} was instantaneously reacted with *500 μM* EGTA. This simulation (Figure 1, Ca trace) shows that $[Ca^{2+}]_{free}$, initially set at 100 μM, would fall at a rate of 600/s producing an ACT with a 1.2 ms hw. This ACT can be produced and visualized by mixing 200 μM Ca^{2+} with an equal volume of the rapid Ca^{2+} indicator MF2 in the presence

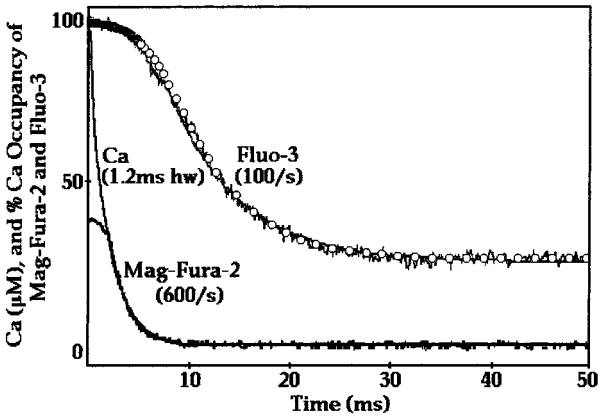

FIGURE 1: Response of the Ca^{2+} indicators mag-fura-2 and fluo-3 to a 1.2 ms half-width artificial Ca^{2+} transient. The traces show the time courses of decrease in $[Ca^{2+}]_{free}$ (Ca^{2+} trace), mag-fura-2 fluorescence (Mag-Fura-2 trace, inverted for comparison), fluo-3 fluorescence (Fluo-3 trace), and a simulation of Ca^{2+} occupancy of Fluo-3 (0), during a 1.2 ms hw artificial Ca^{2+} transient. Ca^{2+} (200 μM) in 10 mM Mops, 90 mM KCl, pH 7.0, was rapidly mixed with an equal volume of the appropriate Ca^{2+} indicator (1 μM) + 1 mM EGTA, in the same buffer at 10 °C. The simulation of fall in $[Ca^{2+}]_{free}$ of this artificial Ca^{2+} transient and of Fluo-3 Ca^{2+} occupancy was modeled using the program KSIM (*19*) and the kinetic parameters described in Table 1. The initial $[Ca^{2+}]$ was set at 100 μM and the initial [EGTA] at 500 μM to mimic the stopped-flow experiments described above. The kinetic parameters in the simulation for the Ca^{2+} off- and on-rates from EGTA of 0.55/s and 1.3×10^6 M^{-1} s^{-1} at 10 °C, respectively, were used. The half-width of the artificial Ca^{2+} transient was measured as the time required for a 50% decrease in $[Ca^{2+}]_{free}$. Control experiments, in which Ca^{2+} + mag-fura-2 or fluo-3 was mixed with buffer + Ca^{2+}, were flat and indicated that ~80% of mag-fura-2 and >95% of fluo-3 were transiently occupied with Ca^{2+} during this artificial Ca^{2+} transient. Mag-fura-2 fluorescence was monitored through a 510 nm broad band-pass filter (Oriel, Stanford, CT) with excitation at 380 nm. Fluo-3 fluorescence was monitored through a 530 nm narrow band-pass filter (Oriel, Stanford, CT) with excitation at 490 nm. Each fluorescence trace represents an average of 5 traces fit with a single-exponential equation (variance < 2×10^{-4}).

of 1 mM EGTA, in a stopped-flow apparatus at 10 °C (Figure 1, Mag-Fura-2 trace). Note that, after mixing, the concentrations of Ca^{2+} and EGTA will be the same as used in the modeling above. Extrapolation of the curve fit to zero time indicated that Ca^{2+} occupied ~80% of the MF2, causing an increase in its fluorescence during the mixing time of the instrument. As the Ca^{2+} was subsequently chelated by EGTA, MF2 fluorescence decreased at a rate of ~600/s which corresponded to the simulated rate of fall in $[Ca^{2+}]$ for this ACT. Thus, the ACT produced when Ca^{2+} is mixed with EGTA can be visualized using MF2 fluorescence. When the higher-affinity Ca^{2+} indicator, Fluo-3, was subjected to the same ACT (Figure 1, Fluo-3 trace), Ca^{2+} initially saturated the indicator, causing an increase in its fluorescence during the mixing time of the instrument. As Ca^{2+} was subsequently chelated by EGTA, there was a lag period before free $[Ca^{2+}]$ was reduced sufficiently to cause dissociation of the Ca^{2+}/Fluo complex and then Fluo-3 fluorescence decreased ~6 times more slowly (100/s) than the MF2 fluorescence and the simulated rate of fall in $[Ca^{2+}]$. A simulation of the Ca^{2+} occupancy of Fluo-3 during this Ca^{2+} transient shows that Ca^{2+} occupancy follows precisely the observed change in Fluo-3 fluorescence. Thus, the rapid Ca^{2+} indicator MF2 accurately reported this ACT while the slower Ca^{2+} indicator fluo-3 responded to the same ACT with a large kinetic delay.

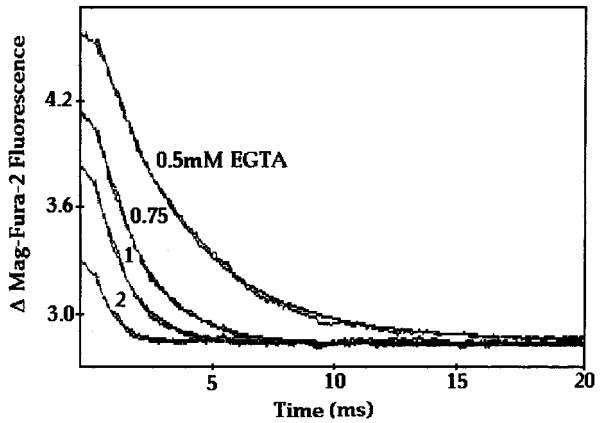

FIGURE 2: Effect of [EGTA] on the half-width of artificial Ca^{2+} transients. Mag-fura-2 fluorescence (traces inverted) was used to follow the time course of the artificial Ca^{2+} transients which were produced when 200 μM Ca^{2+} was rapidly mixed with an equal volume of 1 μM mag-fura-2 in the presence of 0.5, 0.75, 1, or 2 mM EGTA. Experiments were conducted at 10 °C using the buffers described in the legend of Figure 1. Control experiments, in which Ca^{2+} + mag-fura-2 was mixed with buffer + Ca^{2+}, were flat and allowed us to calculate that ~80% of the mag-fura-2 was transiently occupied with Ca^{2+} during each artificial Ca^{2+} transient. Mag-fura-2 fluorescence was monitored as described in the legend of Figure 1. Each trace represents an average of 5 traces fit with a single-exponential equation (variance < 3×10^{-4}).

Effect of [EGTA] on ACT Duration. Figure 2 shows the time courses of several ACTs when Ca^{2+} was rapidly mixed with MF2 in the presence of increasing [EGTA]. When 200 μM Ca^{2+} was mixed with an equal volume of 1 μM MF2 in the presence of 0.5 mM EGTA (Figure 2, 0.5 mM EGTA trace), Ca^{2+} occupied ~80% of the MF2, causing its fluorescence to increase during the mixing time of the instrument. As Ca^{2+} was subsequently chelated by EGTA, MF2 fluorescence decreased at a rate of ~315/s back to its Ca^{2+}-free fluorescence level. Under these conditions, an ACT with an amplitude of 100 μM Ca^{2+} and a hw of 2.2 ms (determined from the extrapolated single-exponential fit to the data) was produced. As the [EGTA] before mixing was successively increased from 0.5 to 0.75, 1 and 2 mM (Figure 2), ACTs of 1.6, 1.2, and 0.6 ms hws were produced. The rate of fall in $[Ca^{2+}]$ in these ACTs increased linearly with increasing [EGTA], as expected for a second-order reaction. At higher [EGTA], more of the Ca^{2+} was chelated during the ~1.6 ms mixing time of the instrument, resulting in less of the decrease in MF2 fluorescence being observed. Thus, ACTs, which vary in duration from 0.6 to 2.2 ms hws, can be generated using various concentrations of the slow Ca^{2+} chelator EGTA. When 200 μM Ca^{2+} was mixed with 1 μM MF2 in the presence of 500 μM EGTA, at 10, 20 and 30 °C, the hw of the ACT decreased from 2.2 to 1.1 to 0.6 ms, respectively (data not shown). Thus, the duration of an ACT generated with EGTA was ~2-fold shorter for each 10° increase in temperature (Q_{10} *of* ~2.0).

Generation of Longer-Duration ACTs Using EDTA. When the Ca^{2+} chelator EDTA is bound to Mg^{2+}, Ca^{2+} cannot bind until Mg^{2+} dissociates. Since Mg^{2+} dissociates from EDTA at ~3/s at 10 °C, Mg^{2+}/EDTA is a slow Ca^{2+} chelator. Therefore, when Ca^{2+} is mixed with Mg^{2+}/EDTA, $[Ca^{2+}]_{free}$ initially rises and then falls as Ca^{2+} displaces Mg^{2+} and binds to EDTA. The very slow Ca^{2+} chelation by Mg^{2+}/EDTA allows the production of ACTs of longer duration than those

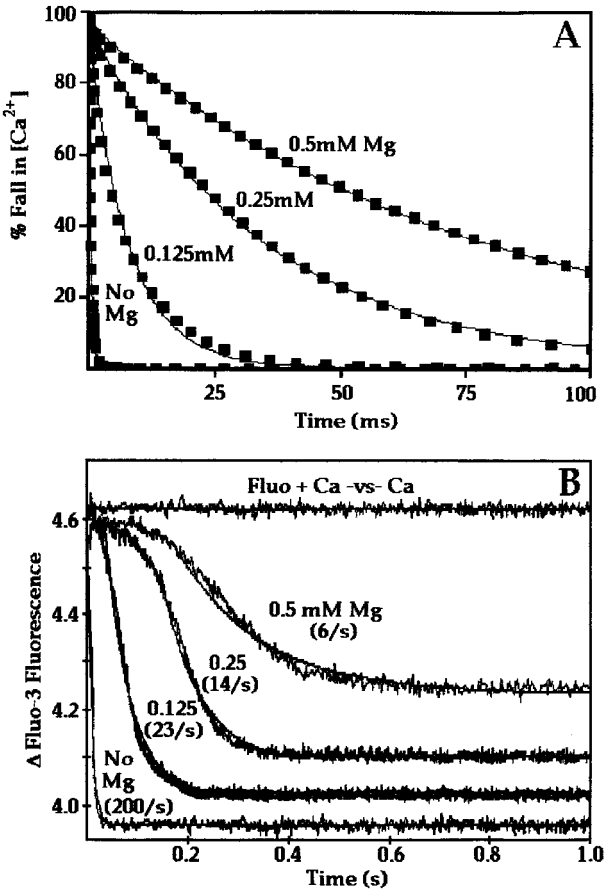

FIGURE 3: Effect of [Mg^{2+}] on the half-width of artificial Ca^{2+} transient created with EDTA. (A) The traces show computer simulations (using KSIM) of the artificial Ca^{2+} transients produced when 10 μM Ca^{2+} was instantaneously reacted with 100 μM EDTA in the absence of Mg^{2+} (no Mg trace), or in the presence of 0.125, 0.25, or 0.5 mM Mg^{2+}. At time = 0, the initial [Mg^{2+}], [EDTA], and [Mg^{2+}/EDTA] were set at the steady-state values for the specific [Mg^{2+}] used, and then 10 μM Ca^{2+} was instantaneously introduced. Ca^{2+} on- and off-rates (2.2×10^7 M^{-1} s^{-1} and 0.7/s, respectively) and Mg^{2+} on- and off-rates (8.75×10^5 M^{-1} s^{-1} and 2.8/s, respectively) from EDTA at 10 °C were used in these simulations. The half-widths of the artificial Ca^{2+} transients were measured as the time required for a 50% decrease in $[Ca^{2+}]_{free}$. (B) The traces show the time course of the decrease in fluo-3 fluorescence that occurs when 20 μM Ca^{2+} was mixed with an equal volume of 1 μM fluo-3 + 200 μM EDTA, in the absence of Mg^{2+} or in the presence of 0.25, 0.5, or 1 mM Mg^{2+} at 10 °C. The [Mg] on each trace represents the [Mg] after the dilution caused by mixing equal volumes. The control experiment, in which Ca^{2+} + fluo-3 was mixed with buffer + Ca^{2+}, was flat and allowed us to calculate that >95% of the fluo-3 was transiently occupied with Ca^{2+} during each artificial Ca^{2+} transient. Buffers and measurement of fluo-3 fluorescence were as described in the legend of Figure 1. Each trace represents an average of 5 traces fit with a single-exponential equation (variance < 9×10^{-5}) after the flat lag phase which represents the Ca^{2+}-saturated state.

produced with EGTA. Figure 3A shows the simulated time course of the fall in $[Ca^{2+}]_{free}$ when 10 μM Ca^{2+} was instantaneously reacted with 100 μM EDTA in the presence of increasing [Mg^{2+}]. This simulation shows that, in the absence of Mg^{2+} (Figure 3A, no Mg trace), an ACT with an amplitude of 10 μM Ca^{2+} and an ~0.3 ms hw was produced. As [Mg^{2+}] was successively increased to 0.125, 0.25, and 0.5 mM, the hw of the ACT progressively increased to 5, 23, and 50 ms, respectively (Figure 3A). Thus, as [Mg^{2+}] was increased from 0 to 0.5 mM, the rate of fall in the Ca^{2+} transient was reduced from ~2300/s to ~14/s, producing an ~165-fold increase in ACT duration.

Fluo-3 was used to visualize the ACT produced with Mg^{2+}/EDTA since fluo-3 fluorescence is not affected by Mg^{2+}. Figure 3B shows fluo-3 fluorescence as a function of time when fluo-3 is subjected to ACTs generated with EDTA in the presence of increasing [Mg^{2+}]. When 20 μM Ca^{2+} was mixed with an equal volume of 1 μM Fluo-3 in the presence of 200 μM EDTA, Ca^{2+} initially occupied ~100% of the fluo-3, causing an increase in its fluorescence during the mixing time of the instrument. As Ca^{2+} was subsequently chelated by EDTA, fluo-3 fluorescence decayed at a rate of ~200/s (3 ms hw) which was ~10 times slower than the simulated rate of fall in [Ca^{2+}] at ~2000/s (0.3 ms hw) in this ACT. As [Mg^{2+}] was increased to 0.125, 0.25, and 0.5 mM (after mixing), Ca^{2+} initially saturated fluo-3, causing an increase in its fluorescence during the mixing time of the instrument. As [Mg^{2+}] was increased, Fluo-3 was saturated with Ca^{2+} for increasing periods of time before Ca^{2+} could displace Mg^{2+} from EDTA and be effectively removed from Fluo-3. Once this occurred, fluo-3 fluorescence (Figure 3B) decreased with hws of ~30 (23/s), 50 (14/s), and 116 ms (6/s) for 0.125, 0.25, and 0.5 mM Mg^{2+}, respectively. As the hw of the simulated ACT increased from 0.3 ms to 5, 23, and 50 ms, fluo-3 reported the decrease in [Ca^{2+}] more accurately with decreasing kinetic delays from ~10- to 2-fold. Due to the competitive binding of Ca^{2+} and Mg^{2+} to EDTA, as the [Mg^{2+}] was increased, EDTA lost some of its capacity to remove Ca^{2+} from fluo-3, and this is reflected by the fact that fluo-3 fluorescence does not return to its Ca^{2+}-free state at higher [Mg^{2+}]. Modeling of the Ca^{2+} occupancy of Fluo-3 by each of these ACT showed that the Ca^{2+} occupancy followed a time course nearly identical to that of the Fluo-3 fluorescence data in Figure 3B (data not shown). Thus, even for the slower Ca^{2+} transients (0.5 mM Mg), the Fluo-3 fluorescence falls at 6/s, ~2 times more slowly than the rate of fall in [Ca^{2+}]. Apparently at higher [Ca^{2+}], the reassociation of Ca^{2+} with Fluo-3 hinders its ability to accurately report even these slower Ca^{2+} transients. These studies show that, at a fixed [EDTA], increasing [Mg^{2+}] produces more of the slow Ca^{2+} chelator Mg^{2+}/EDTA which allows for the creation of ACTs with longer duration (from 0.3 to 50 ms hw).

Using ACTs To Estimate the Ca^{2+} On-Rate to the N-terminal Sites of TnC. TnC-danz is a fluorescently labeled skeletal muscle TnC which undergoes a large increase in fluorescence when its N-terminal regulatory sites bind Ca^{2+} (*18*). TnC-danz has a Ca^{2+} affinity (half-maximal at pCa 5.8) and a Ca^{2+} dissociation rate (~350/s, at 22 °C) similar to those of wild-type TnC (*23*). Figure 4A uses the changes in TnC-danz fluorescence to show the time course of Ca^{2+} binding and dissociation from the N-terminal Ca^{2+}-specific sites of TnC during ACTs of increasing duration at 10 °C. When 200 μM Ca^{2+} was mixed with an equal volume of 2 μM TnC-danz in the presence of 0.75 mM EGTA (Figure 4A, 0.75 mM EGTA trace), a 1.6 ms hw ACT was generated and Ca^{2+} bound and transiently occupied ~100% of the Ca^{2+}-specific regulatory sites of TnC-danz during the mixing time of the instrument. As Ca^{2+} was subsequently chelated by EGTA and removed from TnC-danz, the fluorescence decayed back to its Ca^{2+}-free fluorescence level at a rate of ~95/s. As the [EGTA] before mixing was successively

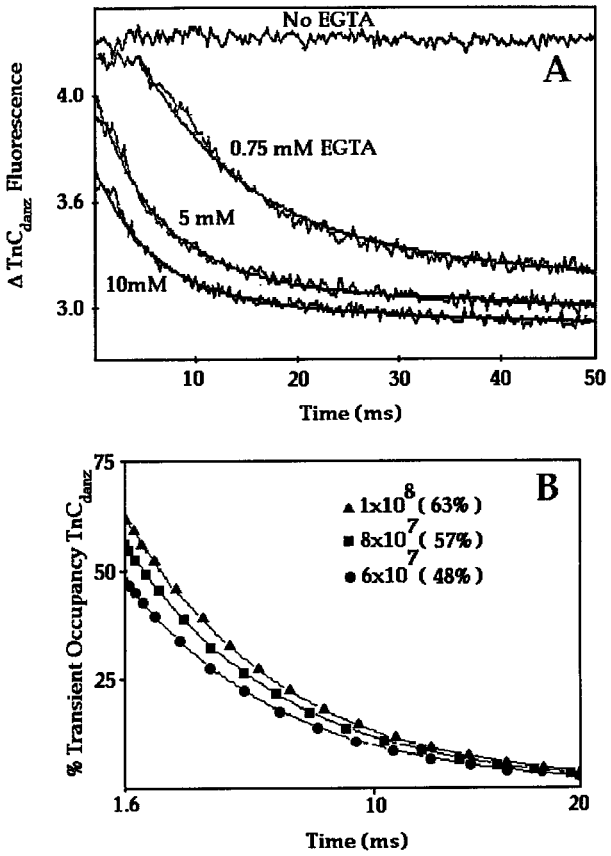

FIGURE 4: Ca^{2+} occupancy of the N-terminal Ca^{2+} specific regulatory sites of troponin C during artificial Ca^{2+} transients of different duration. The traces in panel A show the time courses of decrease in TnC-danz fluorescence when 200 μM Ca^{2+} was mixed with an equal volume of 2 μM TnC-danz in the presence of 0.75, 5, or 10 mM EGTA at 10 °C. The control experiment (no EGTA trace), in which TnC-danz was mixed with buffer + Ca^{2+}, was flat and considered to be 100% occupancy of TnC-danz. TnC-danz fluorescence was monitored through a 510 nm broad band-pass filter (Oriel, Stanford, CT) with excitation at 340 nm. Buffers are those described in the legend of Figure 1. Each trace represents an average of 5 traces fit with a single-exponential equation (variance $< 2 \times 10^{-4}$). Panel B shows a computer simulation of the percent occupancy of the N-terminal sites of TnC in the presence of 5 mM EGTA (after mixing) assuming a Ca^{2+} on-rate of 6×10^7, 8×10^7, or 1×10^8 M^{-1} s^{-1}.

increased from 0.75 to 5 and 10 mM EGTA (Figure 4A), ACTs of 0.21 and 0.1 ms hws were created and Ca^{2+} transiently occupied ~75% and 59% of the N-terminal regulatory sites of TnC-danz, respectively. Furthermore, as [EGTA] was increased from 0.75 to 5 and 10 mM EGTA, Ca^{2+} was chelated and removed from TnC-danz more quickly at rates of 145/s and 160/s, respectively.

Since the percent occupancy of Ca^{2+} bound to the N-terminal of TnC-danz during an ACT of a given duration is directly related to the rate of Ca^{2+} binding to those sites, we were able to estimate the Ca^{2+} on-rate to the regulatory sites of TnC-danz. We used a computer simulation which fixed the Ca^{2+} off-rate from TnC-danz at 160/s (Ca^{2+} off-rate at 10 °C) and let the Ca^{2+} on-rate to TnC-danz vary from 1.0×10^6 to 5.0×10^8 M^{-1} s^{-1} until the modeled transient occupancy and Ca^{2+} dissociation rates approximated the experimental data. The modeling predicts that we should observe the percent occupancies obtained experimentally if the Ca^{2+} on-rate to the Ca^{2+}-specific regulatory sites of TnC-danz is ~$8.7 \pm 2.0 \times 10^7$ M^{-1} s^{-1}, at 10 °C. Figure 4B shows a simulation of the Ca^{2+} occupancy of TnC-danz for the 10 mM EGTA (5 mM after mixing) experiment assuming Ca^{2+} on-rates of 6×10^7, 8×10^7, and 1×10^8 M^{-1} s^{-1}. Modeling with the 6×10^7, 8×10^7, and 1×10^8 M^{-1} s^{-1} on-rates suggested that 48%, 57%, and 63%, respectively, of TnC-danz's N-terminal regulatory sites would be occupied by Ca^{2+} after mixing was complete (1.6 ms). Clearly, even small changes in the assumed Ca^{2+} on-rate can produce large variations in the percent occupancy of the Ca^{2+}-binding sites. A simulation using a Ca^{2+} on-rate of 8.7×10^7 M^{-1} s^{-1} gave an identical 59% occupancy as the actual experimental data with the 10 mM EGTA experiment. Thus, by exposing a Ca^{2+}-binding protein to ACTs of different duration and examining the percent occupancy as a function of Ca^{2+}-transient duration, we can determine the Ca^{2+} on-rate.

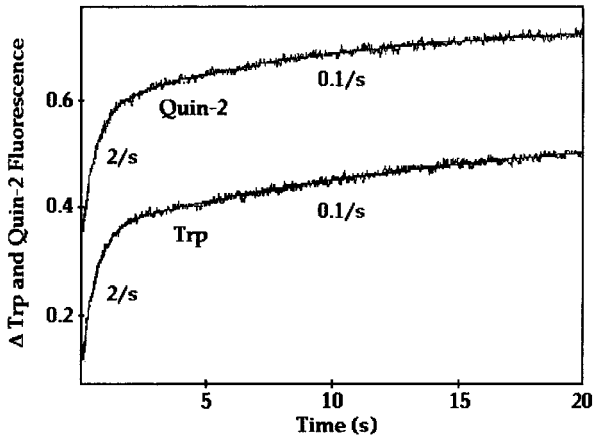

FIGURE 5: The time course of Ca^{2+} and of RS-20 dissociation from the Ca^{2+}/CaM/RS-20 complex. The Quin-2 trace shows the increase in Quin-2 fluorescence that occurs upon Ca^{2+} dissociation from the N- and C-terminals of CaM in the Ca^{2+}/CaM/RS-20 complex. Ca^{2+} (60 μM) + 4 μM CaM + 8 μM RS-20 in 20 mM Hepes, pH 7.0, was rapidly mixed with an equal volume of 200 μM quin-2 in the same buffer at 10 °C. Quin-2 fluorescence was monitored with a 510 nm broad band-pass filter (Oriel, Stanford, CT) with excitation at 330 nm. The trace represents an average of 5 traces fit with a double-exponential equation (variance $< 8 \times 10^{-5}$). The Trp trace shows the increase in RS-20 tryptophan fluorescence that occurs when 75 μM Ca^{2+} + 4 μM CaM + 8 μM RS-20 in 20 mM Hepes, pH 7.0, was rapidly mixed with an equal volume of 20 mM EGTA in the same buffer at 10 °C. RS-20 tryptophan fluorescence was monitored through a UV-transmitting black glass filter with a transmission maxima at 358 nm (UG1 (Oriel, Stanford, CT)) after excitation at 275 nm. When this filter was used, CaM binding to RS-20 produced a decrease in RS-20 fluorescence. The trace is an average of 5 traces fit with a double-exponential equation (variance $< 5 \times 10^{-5}$).

Quin-2 and EGTA Dissociation of Ca^{2+} and RS-20 from the Ca^{2+}/CaM/RS-20 Complex. Ca^{2+} binding to the N- or C-terminal of CaM exposes hydrophobic pockets in both domains that allows CaM to bind target peptides and proteins (for review, see ref *24*). Figure 5 (Quin-2 trace) shows the time course of increase in Quin-2 fluorescence that occurred as 2 mol of Ca^{2+} were removed from both the N-terminal (2/s) and C-terminal (0.1/s) sites of CaM bound to RS-20. Figure 5 (Trp trace) shows the time course of the EGTA-induced increase in RS-20 Trp fluorescence that occurred as RS-20 dissociated from CaM's N-terminal (2/s) and C-terminal (0.1/s). Clearly, RS-20 dissociates from the N- and C-terminals of CaM at the rates at which Ca^{2+} dissociates from the N- and C-terminals of CaM in the Ca^{2+}/CaM/RS-20 complex.

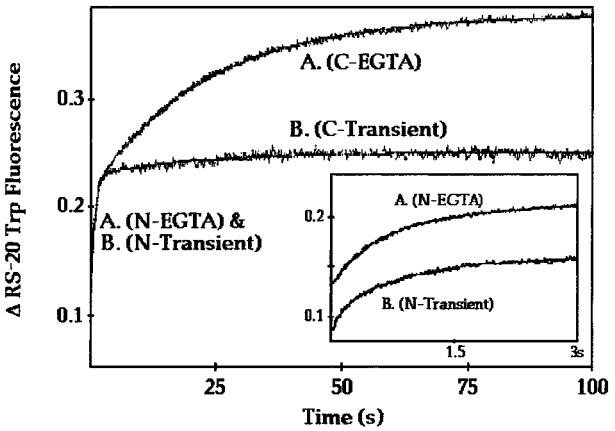

FIGURE 6: The time course of the decrease in Ca^{2+}/CaM/RS-20 Trp fluorescence upon Ca^{2+} chelation by EGTA and after a 1.1 ms half-width artificial Ca^{2+} transient. The time course of the increase in RS-20 tryptophan fluorescence is shown as EGTA dissociates the Ca^{2+}/CaM/RS-20 complex (trace A) or when the complex has been transiently formed by a rapid ACT (trace B). The EGTA-induced increase in RS-20 tryptophan fluorescence (traces labeled A. (N-EGTA) and A. (C-EGTA)) was accomplished by mixing 75 μM Ca^{2+} + 4 μM CaM + 8 μM RS-20 with an equal volume of 20 mM EGTA at 10 °C. The transient occupancy of CaM with Ca^{2+} and RS-20 (trace labeled B. (N-Transient) and B. (C-Transient)) was accomplished by mixing 75 μM Ca^{2+} with an equal volume of 4 μM CaM + 8 μM RS-20 + 1 mM EGTA at 10 °C. The inset shows these two reactions over shorter times with the two traces staggered for comparison. Buffers and measurements of tryptophan fluorescence are described in the legend of Figure 5. All traces are an average of 5 traces fit with a double-exponential equation (variance $< 5 \times 10^{-5}$).

Calmodulin Binding to RS-20 Following a Rapid ACT. The fact that RS-20 Trp fluorescence decreases when it binds to both the N- and C-terminals of CaM allowed us to determine if the N- or C-terminal of CaM could bind to RS-20 during a rapid ACT. Figure 6 shows the EGTA-induced increase in RS-20 Trp fluorescence when EGTA (20 mM) is rapidly mixed with CaM (4 μM) and RS-20 (8 μM) in the presence of 75 μM Ca^{2+}. There is a biphasic increase in RS-20 Trp fluorescence; 50% occurs at 2/s as Ca^{2+} dissociates from the N-terminal (Figure 6, trace A (N-EGTA)) and 50% occurs at 0.1/s as Ca^{2+} dissociates from the C-terminal (Figure 6, trace A (C-EGTA)) of the CaM/RS-20 complex.

By using these changes in RS-20 fluorescence, we were able to determine if either the N- and/or C-terminal of CaM could transiently associate with RS-20 during a rapid ACT. Figure 6 (trace B) shows the change in RS-20 fluorescence that was observed when 75 μM Ca^{2+} was mixed with an equal volume of CaM (4 μM), in the presence of RS-20 (8 μM) and 1 mM EGTA. Following this 1.1 ms hw ACT, Ca^{2+} binds to CaM, and CaM then binds to RS-20 producing a decrease in RS-20 Trp fluorescence during the mixing time of the apparatus. This decrease in fluorescence was followed by a biphasic increase in RS-20 Trp fluorescence. Most (~90%) of this increase in Trp fluorescence occurred as RS-20 dissociated from the N-terminal (Figure 6, trace B (N-Transient)) of CaM at 2/s and the remaining ~10% occurred as RS-20 dissociated from the C-terminal (Figure 6, trace B (C-Transient)) of CaM at 0.1/s. A comparison of the amplitudes of the increase in RS-20 fluorescence that occurred in the ACT experiment (Figure 6, trace B) to the amplitudes of the increase in the EGTA experiment (Figure 6, trace A) suggests that 90% of the N-terminal, but only 10% of the C-terminal, sites of CaM are able to transiently bind to RS-20 during this 1.1 ms hw ACT. Our use of ACT has allowed us to generate a transient kinetic species which could not be observed with conventional stopped-flow techniques; a CaM/peptide complex where only the N-terminal of CaM is bound to Ca^{2+} and to peptide. Furthermore these studies show that during a rapid ACT only the N-terminal of CaM has a fast enough Ca^{2+} on-rate and conformational change to allow it to transiently associate with this target peptide.

CaM Binding to MLCK Following ACTs of Various Duration. Wheat CaM/MIANS exhibits a large fluorescence increase which is specific for its binding to target proteins including MLCK (*17*). This fluorescent CaM allowed us to determine if CaM could bind MLCK after exposure to ACTs of varying duration. Figure 7A uses MF2 fluorescence to visualize the 0.6 ms hw ACT which is produced when 200 μM Ca^{2+} is mixed with an equal volume of 2 mM EGTA (Mag-Fura-2 trace). $[Ca^{2+}]_{free}$ increases during the mixing time of the instrument and decays at a rate of 1200/s. When CaM/MIANS, in the presence of MLCK and EGTA, was exposed to this ACT, CaM/MIANS fluorescence increased at a rate of ~90/s (Figure 7A, CaM_{MIANS} + MLCK trace). There was an ~25 ms delay between peak $[Ca^{2+}]$ and peak CaM/MIANS binding MLCK. In fact, the $[Ca^{2+}]_{free}$ had fallen essentially back to baseline before ~20−30% of the increase in CaM/MIANS fluorescence (Ca^{2+}/CaM/MLCK complex formation) was detected. Since we are exposing CaM and MLCK to a Ca^{2+} transient, the CaM/MIANS/MLCK complex should dissociate after Ca^{2+} has been chelated by EGTA. Figure 7B shows the same trace (2 mM EGTA trace) over longer times (0−5 s). CaM/MIANS fluorescence increased at 90/s and then decreased at a rate of ~1/s. Thus, when subjected to a 0.6 ms hw ACT, CaM/MIANS is able to rapidly and transiently bind MLCK. The no EGTA trace (Figure 7B) shows the CaM/MIANS fluorescence when it is saturated with MLCK. Thus, a 0.6 ms hw ACT allows ~60% of CaM/MIANS to transiently complex with MLCK. Figure 7B also shows the transient binding of CaM/MIANS to MLCK following ACTs with hws of 0.2 and 1.1 ms. A shorter, 0.2 ms hw, ACT (Figure 7B, 5 mM EGTA trace) resulted in ~35% of the CaM/MIANS transiently binding to MLCK, with similar kinetics as the 2 mM EGTA trace. A longer, 1.1 ms hw, ACT (Figure 7B, 1 mM EGTA trace) resulted in ~80% of the CaM/MIANS transiently binding to MLCK, again with similar kinetics. Thus, under the conditions used in these experiments, a ~0.4 ms hw ACT is required for ~50% of the CaM to transiently complex with MLCK. This suggests that the N-terminal of CaM can bind to MLCK with a rate constant of $\sim 6.7 \times 10^7$ M^{-1} s^{-1}, even during very rapid Ca^{2+} transients. These studies also point out an important aspect of CaM's association with its target proteins during cellular Ca^{2+} transients. They suggest that, since CaM binding to a target enzyme can dramatically increase CaM's Ca^{2+} affinity and slow Ca^{2+} dissociation, a CaM/target enzyme complex can exist for seconds after even a very rapid (<1 ms) Ca^{2+} transient has subsided.

Transient Activation of the SR Ca^{2+}/ATPase by ACTs of Different Duration. Watanabe and Inesi (*25*) have previously shown that the Ca^{2+}/ATPase activity of SR vesicles can be followed by the fluorescent nucleotide 2′,3′-*O*-(2,4,6-trini-

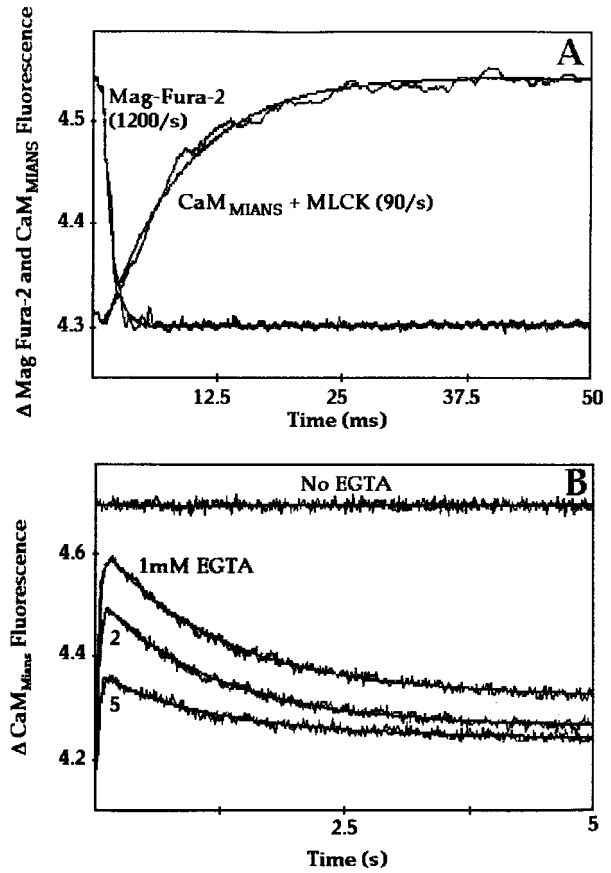

FIGURE 7: The binding of CaM/MIANS to MLCK during artificial Ca^{2+} transients of different duration. Panel A shows the time course of increase in mag-fura-2 fluorescence (Mag-Fura-2 trace, inverted for comparison) and increase in CaM/MIANS fluorescence (CaM-MIANS + MLCK trace) produced by a 0.6 ms half-width artificial Ca^{2+} transient. The transient binding of CaM/MIANS to MLCK was produced by rapidly mixing 200 μM Ca^{2+} with an equal volume of 200 nM CaM/MIANS + 400 nM MLCK + 2 mM EGTA. The Mag-Fura-2 trace was produced by rapidly mixing 200 μM Ca^{2+} with an equal volume of 1 μM mag-fura-2 + 2 mM EGTA. Panel B shows the time course of the rise and fall in CaM/MIANS fluorescence obtained when 200 μM Ca^{2+} was rapidly mixed with an equal volume of 200 nM CaM/MIANS + 400 nM MLCK in the presence of 1, 2, or 5 mM EGTA. CaM/MIANS fluorescence was monitored using a 420−470 nm broad band-pass filter (Oriel, Stanford, CT) with excitation at 320 nm while mag-fura-2 fluorescence was monitored as described in the legend of Figure 1. Experiments were conducted at 10 °C using the buffers described in the legend of Figure 1. The control trace, in which no EGTA (no EGTA trace) was used, shows maximal association of CaM/MIANS with MLCK and is considered 100% binding. Each trace represents an average of 5 traces fit with a double-exponential equation (CaM/MIANS fluorescence) or a single-exponential equation (mag-fura-2 fluorescence) (variance $< 4 \times 10^{-4}$).

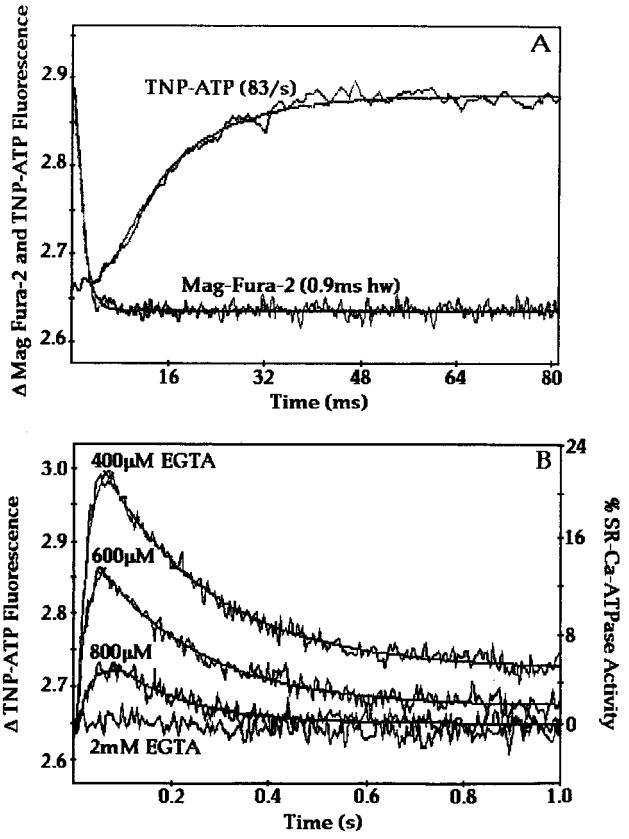

FIGURE 8: Time course of activation of the SR Ca^{2+}/ATPase by artificial Ca^{2+} transients of different duration. Panel A shows the time course of increase in mag-fura-2 fluorescence (Mag-Fura-2 trace, inverted for comparison) and TNP/ATP fluorescence (TNP/ATP trace) by a 0.9 ms half-width artificial Ca^{2+} transient. The transient activation of the SR Ca^{2+}/ATPase was produced by rapidly mixing 200 μM Ca^{2+} with an equal volume of 0.6 mg/mL SR protein in the presence of 10 μM TNP/ATP and 600 μM EGTA. The Mag-Fura-2 trace was produced by rapidly mixing 200 μM Ca^{2+} with an equal volume of 1 μM mag-fura-2 in the presence of 1 mM ATP and 600 μM EGTA. TNP/ATP fluorescence was monitored using a 547 nm band-pass filter (Oriel, Stanford, CT) with excitation at 405 nm. Mag-fura-2 fluorescence was monitored as described in the legend of Figure 1. Each trace represents an average of 8 traces fit with a single-exponential equation (variance $< 2 \times 10^{-4}$). Panel B shows the time course of the rise and fall in TNP/ATP fluorescence (SR Ca^{2+}/ATPase transient activation) obtained when the [EGTA] in the above reactions was decreased from 2 mM to 800, 600, or 400 μM. The control experiment, in which 1.3 mM Ca^{2+} was used to maximally activate the SR Ca^{2+}/ATPase (100%), remained activated for >5 min. Experiments were conducted in 20 mM Tris-Mal and 20% glycerol at 20 °C. Each trace represents an average of 8 traces. Both the increase and decrease in TNP/ATP fluorescence were fit with a single-exponential equation (variance $< 2 \times 10^{-4}$).

trophenyl)/ATP (TNP/ATP). TNP/ATP undergoes a large fluorescence increase which is proportional to the formation of the phosphoenzyme intermediate (E1∼P) when the SR Ca^{2+}/ATPase is activated by Ca^{2+} and Mg^{2+}/ATP (*25*, *26*). This fluorescence decays as E1∼P is inactivated by Ca^{2+} chelation or by ATP depletion. Figure 8A shows a 0.9 ms hw ACT produced when 200 μM Ca^{2+} was mixed with an equal volume of 600 μM EGTA as monitored by the change in MF2 fluorescence (Mag-Fura-2 trace). When vesicles containing the SR Ca^{2+}/ATPase were exposed to this ACT, TNP/ATP fluorescence increased at a rate of ∼83/s (Figure 8A, TNP/ATP trace). There was an ∼32 ms delay between peak [Ca^{2+}] and peak activation of the SR Ca^{2+}/ATPase. In fact, the Ca^{2+} transient had fallen back to baseline before any significant activation of the Ca^{2+}/ATPase occurred. Since this enzyme was activated by a transient increase in Ca^{2+}, it should inactivate after the Ca^{2+} transient subsides. Figure 8B shows the same trace (600 μM EGTA trace) over longer times (0−1 s). TNP/ATP fluorescence increases at 83/s and then decays back to the no Ca^{2+} state (2 mM EGTA trace) at a rate of 4/s. By comparing the Ca^{2+}-induced activation of the SR Ca^{2+}/ATPase obtained in the absence of EGTA and with saturating [Ca^{2+}] (data not shown), we determined that the SR Ca^{2+}/ATPase is transiently activated to ∼14% of its maximal activity by this 0.9 ms hw ACT. Figure 8B

also shows that a shorter-duration, 0.7 ms hw, ACT (Figure 8B, 800 μM EGTA trace) resulted in lower (5%) transient activation of the SR Ca^{2+}/ATPase, while a longer-duration, 1.8 ms hw, ACT (Figure 8B, 400 μM EGTA trace) resulted in greater (22%) transient activation of the enzyme, all with similar kinetics. Thus, the SR Ca^{2+}/ATPase is able to bind Ca^{2+} and become activated after a brief kinetic delay by very rapid ACTs.

DISCUSSION

EGTA has a slow Ca^{2+} on-rate ($1-3 \times 10^6$ M^{-1} s^{-1}) (*21*, *27*) and can be considered a "slow" Ca^{2+} chelator. Thus, when EGTA is rapidly mixed with Ca^{2+} in a stopped-flow apparatus, $[Ca^{2+}]$ rises before it is chelated and this produces an ACT. Since Ca^{2+} binding to EGTA is a second-order reaction, as the [EGTA] is increased, faster ACTs are produced and these can be accurately visualized with the Ca^{2+} indicator MF2 and modeled by computer simulations. By using 200 μM Ca^{2+} and increasing [EGTA], we created ACTs with hws from 16 to 0.1 ms and 100 μM amplitude in a stopped-flow apparatus. The amplitude of the ACT could be increased or decreased by mixing more or less Ca^{2+} with a fixed [EGTA]. By using this method, one can create ACTs with different amplitudes and similar hws.

Because Mg^{2+} must first dissociate from Mg^{2+}/EDTA (at a rate of 3/s at 10 °C) before Ca^{2+} can be chelated, Mg^{2+}/EDTA is an even slower Ca^{2+} chelator than EGTA. Mixing 20 μM Ca^{2+} with 200 μM EDTA and increasing $[Mg^{2+}]$ allowed for the creation of ACTs with hws from 0.3 to 50 ms. When Mg^{2+}/EDTA is used as the Ca^{2+} chelator instead of EGTA, less Ca^{2+} must be used since the Ca^{2+}-chelating potential of EDTA is compromised by the presence of increasing $[Mg^{2+}]$.

We have used these slow Ca^{2+} chelators to create ACTs with different durations and amplitudes by mixing a specific $[Ca^{2+}]$ with a specific concentration of EGTA or Mg^{2+}/EDTA in a stopped-flow apparatus. In this study, we have followed the response of fluorescent Ca^{2+} indicators, Ca^{2+}-binding proteins, and Ca^{2+}-dependent enzymes which were exposed to ACTs of different duration. This has allowed us to characterize the kinetic tuning of these proteins and enzymes to Ca^{2+} transients.

Ca^{2+} indicators such as MF2 and fluo-3 have very rapid ($2-9 \times 10^8$ M^{-1} s^{-1} at 16−22 °C) Ca^{2+} on-rates relative to EGTA (*28*−*30*). Thus, when Ca^{2+} is mixed with these Ca^{2+} indicators in the presence of EGTA, $[Ca^{2+}]$ will rise and bind to the indicators before EGTA. Consistent with this, both indicators underwent an increase in fluorescence during the mixing time of the instrument, followed by a decrease in their fluorescence upon Ca^{2+} chelation. Our studies show that, during a 1.2 ms hw ACT, MF2 accurately reported the rate of fall in $[Ca^{2+}]_{free}$, while fluo-3 reported the fall in $[Ca^{2+}]_{free}$ at an ∼6-fold slower rate. These results are consistent with the fact that fluo-3 has ∼100-fold higher Ca^{2+} affinity and an ∼70-fold slower Ca^{2+} off-rate (∼370/s at 22 °C) compared to MF2 (∼27000/s at 22 °C) (*4*, *29*−*31*). Furthermore, in skeletal muscle, fluo-3 reports the rate of fall in twitch Ca^{2+} transients ∼3−4-fold more slowly than MF2 (*4*, *15*, *32*). Thus, fluo-3 reports the rate of fall of rapid ACTs, and of real Ca^{2+} transients in living muscle, with a kinetic delay because of its slow Ca^{2+} off-rate.

Our studies with skeletal muscle TnC verified that its N-terminal regulatory sites have an ∼60-fold faster Ca^{2+} on-rate than that of EGTA. When TnC was exposed to ACTs of decreasing duration, we observed less transient occupancy of the regulatory sites. Computer simulations of these reactions suggested that the Ca^{2+} on-rate to the regulatory sites of TnC was $\sim 8.7 \pm 2.0 \times 10^7$ M^{-1} s^{-1} at 10 °C. This agrees with our earlier determination of the Ca^{2+} on-rates to the regulatory sites of TnC of $\sim 1 \times 10^8$ M^{-1} s^{-1} at 4 °C (*23*). Thus, by subjecting a Ca^{2+}-binding protein to ACTs of different duration and examining the percent of the protein bound to Ca^{2+} as a function of ACT duration, we can accurately determine the rate of Ca^{2+} binding to that protein. The rapid Ca^{2+} on- and off-rates of the regulatory sites of TnC allow this protein to bind and release Ca^{2+} quickly to initiate contraction and relaxation, respectively (*33*).

We have previously shown that, when a skeletal muscle was loaded with intracellular EGTA and subjected to a twitch, Ca^{2+} could first bind to the regulatory sites of TnC to produce contraction followed by relaxation as Ca^{2+} was chelated by EGTA and resequestered by the SR (*13*). Thus, in our in vitro stopped-flow studies described above, and also in vivo, the regulatory sites of TnC have a much more rapid Ca^{2+} on-rate than that of EGTA, allowing a transient occupancy of the N-terminal regulatory sites and a transient contraction.

We have previously shown that the N-terminal of CaM exhibits ∼70-fold faster rates of Ca^{2+} association than does its C-terminal (1.6×10^8 M^{-1} s^{-1} vs 2.3×10^6 M^{-1} s^{-1}) (*21*). Furthermore, we have shown that the rates of Ca^{2+} dissociation from CaM's N- and C-terminal Ca^{2+}-binding sites in the presence of RS-20 are ∼200 and ∼20 times slower, respectively, than the rates of Ca^{2+} dissociation from these sites in the absence of peptide. Our present studies indicate that Ca^{2+} dissociates from the N-terminal sites of the CaM/RS-20 complex at 2/s and that this is accompanied by peptide dissociation from the N-terminal at 2/s. Similarly, Ca^{2+} dissociates from the C-terminal sites of the CaM/RS-20 complex at 0.1/s, and this is accompanied by peptide dissociation from the C-terminal at the same rate. These results are consistent with the recent findings of Brown et al. (*34*), who demonstrated that high-affinity peptides such as WFF dissociated from the N- and C-terminal of CaM at the same rate that Ca^{2+} dissociated from these domains. Thus, our results of the dissociation of the Ca^{2+}/CaM/RS-20 complex fit into the mechanism of Path A proceeding through steps 1, 5, and 7 as defined by Brown et al. (*34*). In this pathway, Ca^{2+} dissociates from the faster N-terminal of CaM followed by peptide dissociation and then Ca^{2+} dissociates from the slower C-terminal followed by peptide dissociation. While these kinetic studies have defined the Ca^{2+}-exchange rates of CaM in the presence or absence of peptide, they have not allowed investigators to observe how CaM associates and dissociates with target peptides or proteins when exposed to a Ca^{2+} transient. Our present studies, with the use of ACTs, show that, in response to a 1.1 ms hw ACT, only the faster N-terminal of CaM was able to significantly bind Ca^{2+} and expose its hydrophobic pocket rapidly enough to bind RS-20. The C-terminal domain of CaM binds Ca^{2+} too slowly to allow peptide binding following a rapid Ca^{2+} transient.

When CaM/MIANS and MLCK were exposed to ACTs of various duration, we found that ~50% of CaM/MIANS could complex with MLCK during a very brief (~0.5 ms hw) ACT. Thus, CaM is able to bind to MLCK after exposure to rapid ACTs (0.2−1.1 ms hws). The data are consistent with the interpretation that we are observing the N-terminal of CaM/MIANS binding to MLCK since (1) the MIANS label is covalently attached to the N-terminal (Cys 28) of CaM (*17*); (2) the ACTs we used are too fast to allow significant C-terminal Ca^{2+} binding to occur because the C-terminal of CaM has an ~70-fold slower Ca^{2+} on-rate than the N-terminal (2.3×10^6 M^{-1} s^{-1} vs 1.6×10^8 M^{-1} s^{-1}) (*21*); and (3) only the N-terminal of CaM was able to bind to the smooth muscle MLCK-binding peptide, RS-20, during similar rapid ACTs. The observed rate of CaM binding to MLCK at ~90/s is comparable to the rapid (65/s, at 23 °C) increase in Trp fluorescence that occurs when CaM binds to skeletal muscle MLCK (*35*). Modeling of the transient binding of CaM/MIANS to MLCK predicted the association rate of the complex to be $\sim 6.7 \times 10^7$ M^{-1} s^{-1}, consistent with previously determined association rates of CaM for smooth and skeletal muscle MLCK of $2.8 \times 10^7 - 4.6 \times 10^7$ M^{-1} s^{-1}, respectively (*17, 36*). As EGTA dissociated the CaM/MLCK complex, we observed a dissociation rate of ~1/s for all of the ACTs at 10 °C. This slow dissociation rate is comparable to our earlier finding that EGTA dissociates the CaM/MLCK complex at 2−3/s at 22 °C (*17, 35*).

Our data indicates that, even during a rapid ACT, with a much shorter hw than those observed in smooth or skeletal muscle, CaM's N-terminal can bind Ca^{2+} quickly and then rapidly associate with MLCK. The high Ca^{2+} affinity of the C-terminal lobe of CaM complexed to CaM-binding proteins may allow the C-terminal of CaM to be bound to proteins, like MLCK, at resting concentrations of cellular Ca^{2+} (*21, 34, 37*). If this is the case, and since binding of both the N- and C-terminal lobes of CaM to target proteins is required for enzyme activation (*38*), then rapid binding of Ca^{2+} to the N-terminal sites of CaM during a Ca^{2+} transient may allow the N-terminal of CaM to bind and activate target proteins such as MLCK. Subsequently, the fall in $[Ca^{2+}]$ would cause the N-terminal of CaM to dissociate from the target protein first, since the N-terminal of CaM has an ~20-fold faster Ca^{2+} off-rate than the C-terminal when complexed with MLCK (2/s vs 0.1/s (*21*)). Consistent with this interpretation, EGTA inactivated the CaM/MLCK complex at a rate of ~1/s (*39*). Thus, Ca^{2+} dissociation from the N-terminal sites of CaM in the Ca^{2+}/CaM/MLCK complex is presumably responsible for enzyme inactivation as $[Ca^{2+}]$ falls (*21*). This implies that the faster, lower-affinity N-terminal Ca^{2+}-binding sites of CaM may be the regulatory sites of this protein, analogous to the rapid N-terminal Ca^{2+}-binding sites of TnC which regulate cardiac and skeletal muscle contraction and relaxation (*40*).

The SR Ca^{2+}/ATPase was half-maximally activated in a transient fashion by an ~5 ms hw ACT. The ability of the SR Ca^{2+}/ATPase to respond to rapid ACTs is consistent with a fast Ca^{2+} on-rate ($\sim 2 \times 10^7 - 4 \times 10^8$ M^{-1} s^{-1}) to this enzyme (*41, 42*). The rate of increase in TNP/ATP fluorescence that we observe at ~83/s at 20 °C is consistent with earlier reports of Ca^{2+}-dependent enzyme activation at 85−150/s under conditions of saturating TNP/ATP and/or ATP at ~25 °C (*26, 43*). It was interesting that the ACT had fallen back to baseline before the enzyme exhibited any activation. There was an ~30 ms delay between the time required for peak Ca^{2+} and peak activation of the SR Ca^{2+}/ATPase, consistent with a model of the catalytic cycle of the SR Ca^{2+}/ATPase proposed by Inesi et al. (*44*). This kinetic delay, between the rise in cytosolic Ca^{2+} and enzyme activation, may provide a mechanism which would allow Ca^{2+} to bind to the N-terminal regulatory site(s) of TnC and initiate contraction before the SR Ca^{2+}/ATPase could be activated to resequester Ca^{2+} and facilitate relaxation.

Our rates of EGTA-induced SR Ca^{2+}/ATPase inactivation (~4/s) are comparable to previous studies in which the enzyme was inactivated by EGTA at ~1.8/s at 25 °C (*26*). EGTA inactivates the SR Ca^{2+}/ATPase by chelating the $[Ca^{2+}]_{free}$ and preventing the enzyme from binding more Ca^{2+}. The rate of inactivation of the SR Ca^{2+}/ATPase that we observe (4/s) may correspond to the rate (~3/s) at which prebound, occluded Ca^{2+} is translocated into the lumen of SR Ca^{2+}/ATPase vesicles (*45*). After the translocation of Ca^{2+}, the SR Ca^{2+}/ATPase inactivates since the pump can no longer bind free Ca^{2+} due to EGTA chelation. These studies are consistent with our observed decrease in TNP/ATP fluorescence occurring at the rate of SR luminal Ca^{2+} release. Our data are consistent with theories which suggest that, as soon as Ca^{2+} is released in a skeletal muscle cell, the SR Ca^{2+}/ATPase can initially bind Ca^{2+}, and with a kinetic delay, actively begin to sequester Ca^{2+} (*42*).

There are certain limitations to the use of ACT that should be mentioned. (1) Since the ability of both EDTA and EGTA to chelate Ca^{2+} is affected by pH, it is important to have sufficient buffer to maintain the desired pH. (2) The Ca^{2+}-exchange rates of EGTA increase with temperature, and we determined that the hw of an ACT generated with EGTA exhibits a Q_{10} of ~2. (3) While all of our ACT were generated with [EGTA] in excess of [Ca], it should be noted that, as the $[Ca^{2+}]$ approaches the [EGTA], the duration of the ACT increases as the chelating potential of EGTA is reduced. (4) When Mg/EDTA is used as the chelator it is important to recognize that at higher [Mg], EDTA will be a less efficient chelator and lower $[Ca^{2+}]$ should be used to produce the ACT. (5) As with all stopped-flow experiments, the amount of the reaction that can be observed is dependent on the mixing time of the instrument and the extent of the changes in absorption or fluorescence that occurs with the event being studied. For all of these reasons we recommend that the actual ACT which is being generated be first visualized by rapid Ca^{2+} indicators such as Mag-fura-2. After verification of the ACT which is being generated, any protein's response to that ACT could be determined.

We have exposed several Ca^{2+} indicators, Ca^{2+}-binding proteins, and a Ca^{2+}-dependent enzyme to ACTs of various durations and observed their transient binding of Ca^{2+}, complex formation, and activation. This has allowed us to characterize the response of these Ca^{2+}-dependent proteins to Ca^{2+} transients of varying amplitude and duration. We show that their response to and their "memory" of these Ca^{2+} transients are dictated by their Ca^{2+}-exchange kinetics. Proteins with higher Ca^{2+} affinity and slower Ca^{2+} off-rates exhibit a longer memory for Ca^{2+} and can remain active long after the Ca^{2+} transients have subsided. Furthermore, by characterizing the response of these proteins to ACTs, we can predict with greater certainty, how they would respond

to natural Ca^{2+} transients to regulate cellular phenomena. Future applications of these ACTs should further increase our understanding of how different Ca^{2+}-dependent phenomena are controlled by cellular Ca^{2+} transients and by the Ca^{2+} tuning of Ca^{2+}-binding proteins and enzymes.

REFERENCES

1. Clapham, D. E. (1995) *Cell 80*, 259−268.
2. Falke, J. J., Drake, S. K., Hazard, A. L., and Peersen, O. B. (1994) *Q. Rev. Biophys. 27*, 219−290.
3. Llinas, R., Sugimori, M., and Silver, R. B. (1995) *Neuropharmacology 34*, 1443−1451.
4. Zhao, M., Hollingworth, S., and Baylor, S. M. (1996) *Biophys. J. 70*, 896−916.
5. Gilbert, E. K., Weaver, B. A., and Rembold, C. M. (1991) *FASEB J. 5*, 2593−2599.
6. Sargeant, P., and Sage, S. O. (1994) *Pharmacol. Ther. 64*, 395−443.
7. Ghosh, A., and Greenberg, M. E. (1995) *Science 268*, 239−247.
8. Trump, B. F., and Berezesky, I. K. (1995) *FASEB J. 9*, 219−228.
9. Niki, I., Yokohura, H., Sudo, T., Kato, M., and Hidaka, H. (1996) *J. Biochem. (Tokyo) 120*, 685−698.
10. Kurihara, S., and Konishi, M. (1987) *Pfluegers Arch. 409*, 427−37.
11. Dolmetsch, R. E., Lewis, R. S., Goodnow, C. C., and Healy, J. I. (1997) *Nature 386*, 855−858.
12. Haiech, J., Derancourt, J., Pechere, J., and Demaille, J. G. (1979) *Biochemistry 18*, 2752−2758.
13. Johnson, J. D., Jiang, Y., and Flynn, M. (1997) *Am. J. Physiol. 272*, C1437−C1444.
14. Xu, Y., Shao, Q., and Dhalla, N. S. (1997) *Mol. Cell. Biochem. 172*, 149−157.
15. Jiang, Y., Johnson, J. D., and Rall, J. A. (1996) *Am. J. Physiol. 270*, C411−C417.
16. Adler, E. M., Augustine, G. J., Duffy, S. N., and Charlton, M. P. (1991) *J. Neurosci. 11*, 1496−1507.
17. Kasturi, R., Vasulka, C., and Johnson, J. D. (1993) *J. Biol. Chem. 268*, 7958−7964.
18. Johnson, J. D., Collins, J. H., and Potter, J. D. (1978) *J. Biol. Chem. 253*, 6451−6458.
19. Ngai, P. K., Carruthers, C. A., and Walsh, M. P. (1984) *Biochem. J. 218*, 863−870.
20. Elter, S., and Inesi, G. (1972) *Biochim. Biophys. Acta 282*, 174−179.
21. Johnson, J. D., Snyder, C., Walsh, M. P., and Flynn, M. (1996) *J. Biol. Chem. 271*, 761−767.
22. Dantzig, J. A., Goldman, Y. E., Millar, N. C., Lacktis, J., and Homsher, E. (1992) *J. Physiol. 451*, 247−278.
23. Johnson, J. D., Nakkula, R. J., Vasulka, C., and Smillie, L. B. (1994) *J. Biol. Chem. 269*, 8919−8923.
24. Rhoads, A. R., and Friedberg, F. (1997) *FASEB J. 11*, 331−340.
25. Watanabe, T., and Inesi, G. (1982) *J. Biol. Chem. 257*, 11510−11516.
26. Bishop, J. E., Johnson, J. D., and Berman, M. C. (1984) *J. Biol. Chem. 259*, 15163−15171.
27. Smith, P. D., Liesegang, G. W., Berger, R. L., Czerlinski, G., and Podolsky, R. J. (1984) *Anal. Biochem. 143*, 188−195.
28. Naraghi, M. (1997) *Cell Calcium 22*, 255−268.
29. Lattanzio, F. A., and Bartschat, D. K. (1991) *Biochem. Biophys. Res. Commun. 177*, 184−191.
30. Escobar, A. L., Velez, P., Kim, A. M., Cifuentes, F., Fill, M., and Vergara, J. L. (1997) *Pfluegers Arch. 434*, 615−631.
31. Ogden, D., Khodakhah, K., Carter, T., Thomas, M., and Capiod, T. (1995) *Pfluegers Arch. 429*, 587−591.
32. Caputo, C., Edman, K. A. P., Lou, F., and Sun, Y.-B. (1994) *J. Physiol. 478*, 137−148.
33. Johnson, J. D., Charlton, S. C., and Potter, J. D. (1979) *J. Biol. Chem. 254*, 3497−3502.
34. Brown, S. E., Martin, S. R., and Bayley, P. M. (1997) *J. Biol. Chem. 272*, 3389−3397.
35. Johnson, J. D., Holroyde, M. J., Crouch, T. H., Solaro, R. J., and Potter, J. D. (1981*) J. Biol. Chem. 256*, 12194−12198.
36. Bowman, B. F., Peterson, J. A., and Stull, J. T. (1992) *J. Biol. Chem. 267*, 5346−5354.
37. Bayley, P. M., Findlay, W. A., and Martin S. R. (1996) *Protein Sci. 5*, 1215−1228.
38. Persechini, A., and Kretsinger, R. H. (1988) *J. Biol. Chem. 263*, 12175−12178.
39. Stull, J. T., Nunnally, M. H., and Michnoff, C. H. (1986) *The Enzymes*, Academic Press, Orlando, FL.
40. Robertson, S. P., Johnson, J. D., and Potter, J. D. (1981) *Biophys. J. 34*, 559−569.
41. Cantilina, T., Sagara, Y., and Inesi, G. (1993) *J. Biol. Chem. 268*, 17018−17025.
42. Inesi, G., Kurzmack, M., and Lewis, D. (1988) *Methods Enzymol. 157*, 154−190.
43. Froehlich, J. P., and Taylor, E. W. (1975) *J. Biol. Chem. 250*, 2013−2021.
44. Inesi, G., Kurzmack, M., Coan, C., and Lewis, D. E. (1980) *J. Biol. Chem. 255*, 3025−3031.
45. Orlowski, S., and Champeil, P. (1991) *Biochemistry 30*, 11331−11342.

BI982495Z